Available online at www.sciencedirect.com
ScienceDirect
Trans. Nonferrous Met. Soc. China 21(2011) 830−835
Transactions of Nonferrous Metals Society of China
www.tnmsc.cn

Effects of processing route on texture and mechanical properties of WZ62 alloy

SHI Bin-qing, CHEN Rong-shi, KE Wei

State Key Laboratory for Corrosion and Protection, Institute of Metal Research, Chinese Academy of Sciences, Shenyang 110016, China

Received 25 September 2010; accepted 20 December 2010

Abstract: Mg-6.6%Y-2.3%Zn (WZ62, mass fraction) magnesium alloys were fabricated by equal-channel-angular-extrusion (ECAE), and ECAE followed by forging processing, respectively. The "necklace" structure that is composed of fine recrystallized and coarse initial grains was found. The process of dynamic recrystallization (DRX) is associated with the strain localization. With increasing ECAE passes, the tensile test results reveal that both the strength and elongation are enhanced. A typical non-basal texture component in the (0002) pole figures with tilted peaks at about 45° was observed. After ECAE followed by forging processing, the strength increases greatly with sacrificed ductility. That is attributed to the change in the texture: the majority of basal planes is rotated to be normal to the normal direction. The non-basal texture induced by ECAE is modified by the secondary forging processing.

Key words: magnesium alloy; Mg-Y-Zn alloy; equal-cannel-angular-extrusion (ECAE); texture control

1 Introduction

Recently, Mg-Y-Zn alloys have been given tremendous attention due to high strength at room and elevated temperatures. A high yield strength of 610 MPa and a relative high tensile ductility of 5% at room temperature, and high yield strength more than 380 MPa at 473 K were reported for the extremely fine-grained (d =100−150 nm) rapidly solidified powder metallurgy (RS P/M), MgY_2Zn_1 (mole fraction, %) alloys exhibit high strength at elevated temperature[1]. Later, some 6H-type ABCBCB long period ordered (LPO) structure was reported in this alloy[2]. According to the research by LUO and ZHANG[3] and ITOI et al[4], the structure in the Mg-Y-Zn cast alloy is better described as an 18R LPO structure. However, recently it is demonstrated that the structure of $Mg_{12}YZn$ phase in the above researches is 14H structure[5]. Afterwards, great deals of researches have been reported on the mechanical properties of bulk Mg-RE (rare element)-TE (transition element) alloys with LPO structure. The $Mg_{93.5}Y_{3.5}Zn_3$ (mole fraction, %) wrought alloy[6] was developed with excellent tensile yield strength of 440 MPa, ultimate strength of 492 MPa, and elongation of 6%. Additionally, a MgY_2Cu_1 (mole fraction, %) magnesium alloy after extrusion also exhibited excellent mechanical properties at room and elevated temperatures[7]. The high tensile strength should be attributed to the refined microstructure and strengthening effect from the second phase with long period ordered structure (LPSO) structure.

Equal-channel-angular extrusion (ECAE) has been generally accepted as an effective method to refine the microstructure in magnesium alloys. However, the strength of magnesium alloys processed by ECAE was decreased rather than enhanced, which was attributed to the texture softening effect[8]. In this work, a processing route combined with ECAE and forging was firstly developed to modify the non-basal texture generated by ECAE. A WZ62 alloy (Mg-6.6%Y-2.3%Zn, mass fraction) with LPO structure was chosen and performed by ECAE and ECAE followed by forging processing, respectively. Tensile testing at room temperature was carried out on WZ62 alloy produced by different processing routes; in addition, the influence of texture on the mechanical properties was also investigated.

2 Experimental

The analyzed chemical composition of WZ62 alloy is Mg-6.6%Y-2.3%Zn (mass fraction). The cast

Corresponding author: CHEN Rong-shi; Tel: +86-24-23926646; Fax: +86-24-23894149; E-mail: rschen@imr.ac.cn
DOI: 10.1016/S1003-6326(11)60789-9

ingot was homogenized at 535 °C for 21 h. Then billets with dimensions of 12 mm×12 mm×110 mm for ECAE processing were machined from the heat-treated ingot. The billets were conducted to ECAE at 400 °C with molybdenum disulphide (MoS_2) as lubricant; the processing temperature was controlled in ±2 °C. The route for ECAE processing was Bc, that is, samples were rotated 90° about the billet axis between passes.

After ECAE, subsequent forging processing was performed on the extrusion direction (ED)/transverse direction (TD) surface of samples that were machined from ECAEed billets. The forging temperature was 350 °C. The reduction and processing speed was about 60% and 1 mm/min, respectively. After many trials, the samples produced by one pass-ECAE and forging processing were cracked by using this forging method, so these samples would not be investigated in this study.

Tensile specimens were machined into dog-bone shape with 6 mm in gauge length and 2 mm×3 mm in cross-section. Tensile tests were conducted on the Sans type tensile testing machine at an initial strain rate of $1\times10^{-3}s^{-1}$ at room temperature. The stress direction was along the extrusion direction of the ECAEed samples and perpendicular to the forging direction of the forged samples. Hereafter, ED, TD, ND and FD denote the extrusion, transverse, normal and forging direction, respectively.

Microstructure observation was performed on an optical microscope and a Philip XL30 ESEM-FEG/EDAX scanning electron microscope. The phases were analyzed by the SEM equipped with an energy-dispersive X-ray (EDX) spectroscopy analysis system and identified by X-ray diffractometry using a monochromatic Cu K_α radiation. Texture analysis was carried out on a RigakuD/max 2400 X-ray diffractometer using Cu K_α radiation with the sample tilt angle ranging from 0°−70°. Texture analysis of the samples processed by different routes was performed using the Schultz reflection method by X-ray diffractometry. Calculated pole figures were obtained with the DIFFRAC^{plus} TEXEVAl software, using the measured incomplete $\{0002\}$, $\{10\bar{1}0\}$ and $\{10\bar{1}1\}$ pole figures.

3 Results and discussion

3.1 Evolution of "necklace" structure

Figures 1(a) and (b) show the microstructure of WZ62 alloy in the as-cast and solid solution treatment states, respectively. The microstructure of WZ62 alloy is composed of α-Mg and block eutectic phase. Figure 2(a) exhibits the EDS spectra of the eutectic phase, whose composition is $Mg_{87.49}Y_{6.44}Zn_{5.77}$ (mole fraction, %). Combined with the XRD analysis, the phase is identified as $Mg_{12}YZn$ phase. The structure of the $Mg_{12}YZn$ phase is LPSO, and some peaks are close to those of

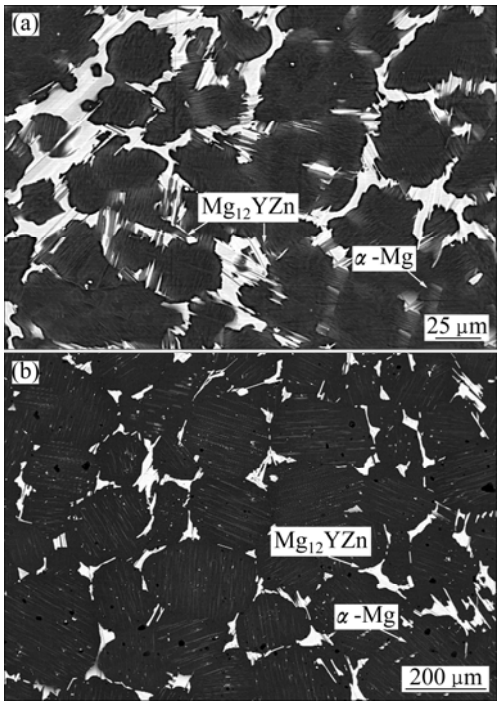

Fig.1 SEM images of WZ62 alloy: (a) As-cast; (b) Solid solution treatment state at 535 °C for 21 h

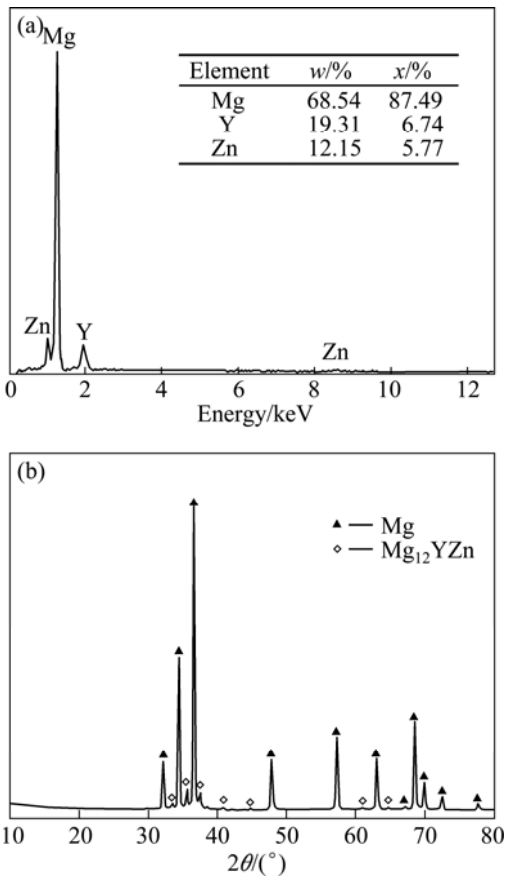

Fig.2 EDS spectrum of eutectic phase (a) and XRD pattern of as-cast WZ62 alloy (b)

magnesium in the XRD pattern[3]. After solid solution heat treatment at 535 °C for 21 h, the $Mg_{12}YZn$ phase dissolves partly into the matrix (Fig.1(b)).

Optical micrographs of WZ62 alloy fabricated by ECAE or ECAE followed by forging processing are shown in Fig.3. In Fig.3, E1 denotes one pass-ECAE; E2F stands for two passes-ECAE followed by forging processing. The samples processed by the other routes in this study were also nominated in this way. The microstructure of specimen processed by E1 is shown in Fig.3(a). Twins are observed in some grains and remaining $Mg_{12}YZn$ phase is found at some grain boundaries. After E2, as shown in Fig.3(b), most of the initial equiaxed grains are elongated and some fine DRX grains are found to form clusters at grain boundaries. The measured size of the DRX grains is less than 5 μm (from rectangle region in Fig.3(b)).

Figure 3(c) exhibits the microstructure after E3 processing. Slip bands are clearly observed in most of the initial grains and some elongated grains break into fragments, as marked with the rectangle in Fig.3(c). Figure 3(d) shows the amplificatory microstructure of the elongated grain with serrated boundaries marked with dark lines. Dense slip bands are observed near the region where new DRX grains nucleate. It should be noted that there exists similarity in morphology between the slip bands or shear bands (indicated by the black arrows) and DRXed regions (marked with the rectangles). That is also the case for the specimens processed by E2F and E3F, as shown in Figs.3(d) and (e), respectively. Consequently, it can be imaged that the process of DRX is associated with strain localization and is manifested as the occurrence of dense slip bands or shear bands.

The microstructures in Fig.3 show the typical "necklace" structure: initial coarse grains are surrounded by fine recrystallized grains. The initiation of DRX is preceded by growing fluctuations of the grain boundary shape. Serrations and bulges develop, and eventually

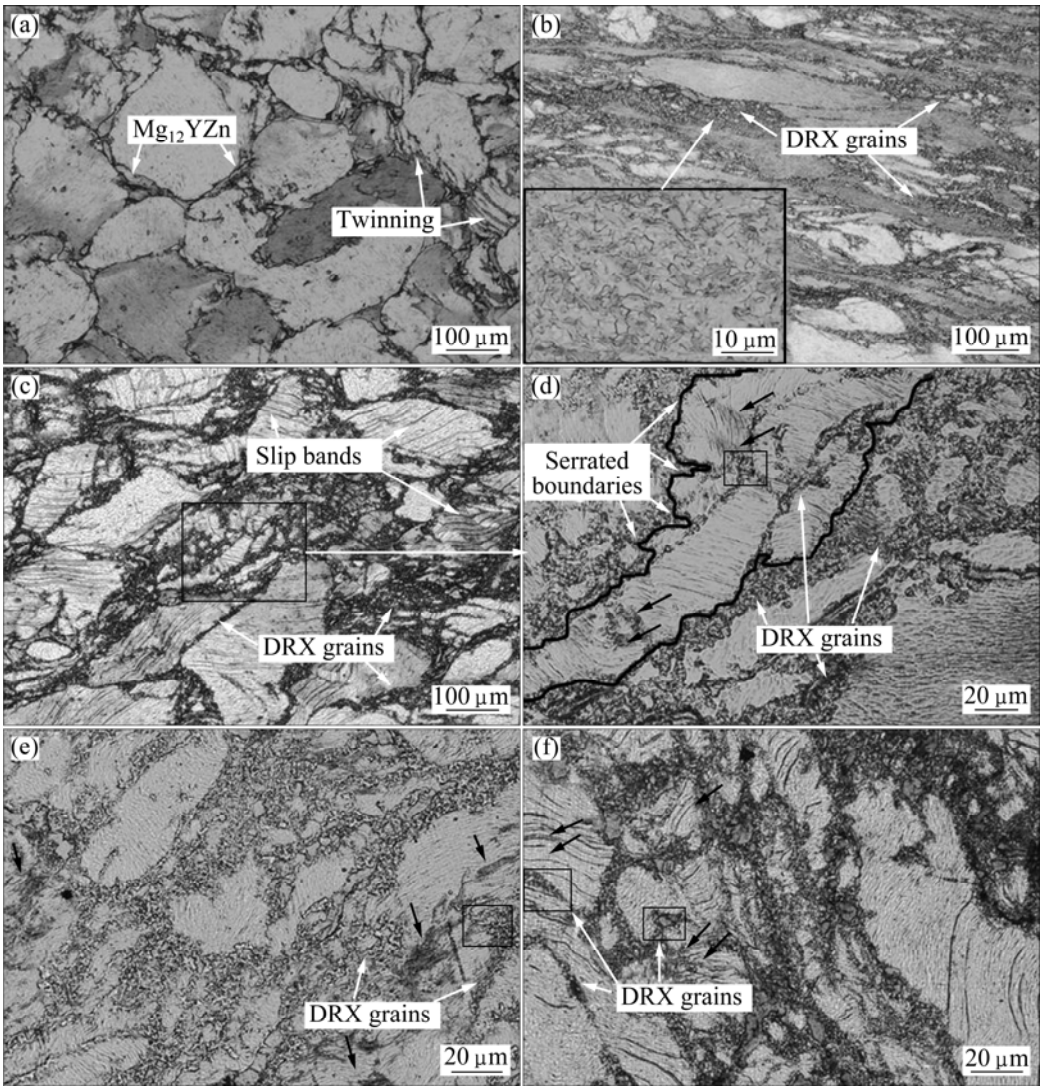

Fig.3 Microstructures of WZ62 alloy processed by different processing routes: (a) E1; (b) E2; (c) E3; (d) Amplificatory part of rectangle in Fig.(c); (e) E2F; (f) E3F (The observed surfaces of specimens processed by E1-E3 are parallel to ED/TD surface; the observed surfaces of those processed by E2F or E3F are perpendicular to FD.)

new grains are generated along these prior grain boundaries[9]. Actually the formation of the "necklace" structure is associated with many factors, such as strain capacity[9], temperature and strain rate[10−11]. This structure has been reported in many materials, especially in those with low surface fault energy (SFE), such as magnesium and nickel alloys[9−11].

The mechanism of DRX analyzed by McQUEEN and KONOPLEVA[13] can be used to explain the formation of "necklace" structure in this study: twinning takes place at low strains to reorient grains not suit for slip. As strain reaches a sufficiently high level, DRX grains nucleate at the locations where high misorientations have been created by accumulation of dislocations, i.e. where slip has occurred on several slip system (near grain boundaries and twins)[13]. That can also account for the observed twining (Fig.3(a)) and dense slip bands in association with DRX region (Figs.3(d) and (f)). In addition, the recrystallized fine grains were more favorable for basal slip than the initial coarse grains[14]. When the specimens are stressed in serious deformation, strain favorably localized within the DRX region. However, the initial coarse grains are hard to be refined, unless enough strain is induced by mechanical processing.

3.2 Mechanical properties and change in texture

Figure 4 shows the typical tensile curves of the WZ62 alloy fabricated by different processing routes. The tensile mechanical properties including ultimate tensile strength (UTS), yield strength (YS) and elongation-to-failure are listed in Table 1. In contrast to the solution treated state (T4), both the UTS and YS were increased markedly after E1, while the elongation-to-failure decreased from 12.3% to 5.9%. With accumulated ECAE passes, all the tensile properties including the strength and elongation-to-failure were enhanced. It is worth noting that after forging processing

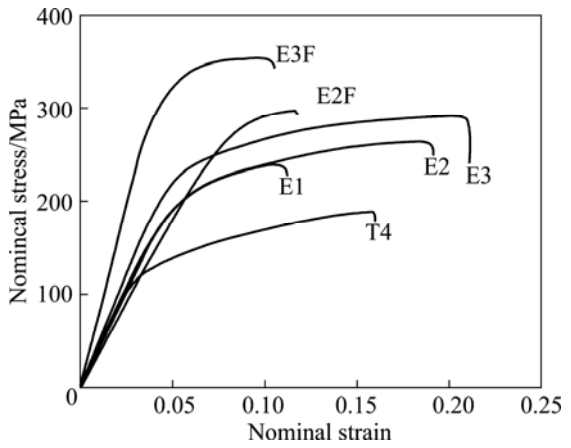

Fig.4 Typical tensile curves of WZ62 alloy produced by different processing routes

Table 1 Mechanical properties of WZ62 alloy

State	UTS/MPa	YS/MPa	Elongation-to-failure/%
T4	187.3	97.2	12.3
E1	239.1	154.0	5.9
E2	263.3	176.4	13.1
E3	298.7	185.5	16.3
E2F	296.5	228.6	4.2
E3F	352.7	280.1	6.2

the strength was greatly improved; the UTS of the specimens processed by E2F and E3F increased from 263.3 to 296.5, 298.7 to 352.7 MPa, respectively.

The variation in mechanical properties of the tensile samples performed by different processing routes should be associated with the change in texture. The (0002) pole figures after E1, E2 and E3 are shown in Figs.5(a)−(c), respectively. After E1, the peak intensity oriented at approximately 45° to the nominal direction with two secondary peaks nearly parallel to the transverse axis. This texture component places the basal planes nearly coincident with the shear plane in the ECAE die. Subsequent pass serves to deflect the peak intensity to about 70° along the transverse axis. After E3, the peak intensity is inclined to about 45° to the nominal direction. Notice that E3 also orients the secondary peaks to 45° to the transverse axis, compared with that of E1 and E2. It can be predicted that the majority of the basal planes lie at approximately 45° of the TD/ND plane, which is the consequence of the processing route Bc.

Though the distribution and shape of the contour lines in the (0002) pole figures of the samples processed by ECAE for different passes seem to be different, there exist two common features in essence. One is that the peak intensities in the (0002) pole figures are about three times that of a random distribution (MRD); the other is that the peaks are oriented approximate at 45° or higher angle to extrusion direction. That is, the texture component is typical non-basal texture induced by ECAE processing.

Figures.5(d) and (e) show the (0002) pole figures of the samples fabricated by E2F and E3F, respectively. The majority of basal planes are oriented to be perpendicular to the normal direction with the maximum intensities of about seven times that of MRD; additionally, the texture is comparably intense. That is in contrast to the (0002) pole figures of E2 and E3 shown in Figs.5(b) and (c). The measured textures after forging processing in the present study are similar to the typical basal textures after forging processing[15]. That also indicates that the initial textures induced by ECAE make only a limited contribution to the ultimate texture, which should be dominated by the secondary forging processing. The

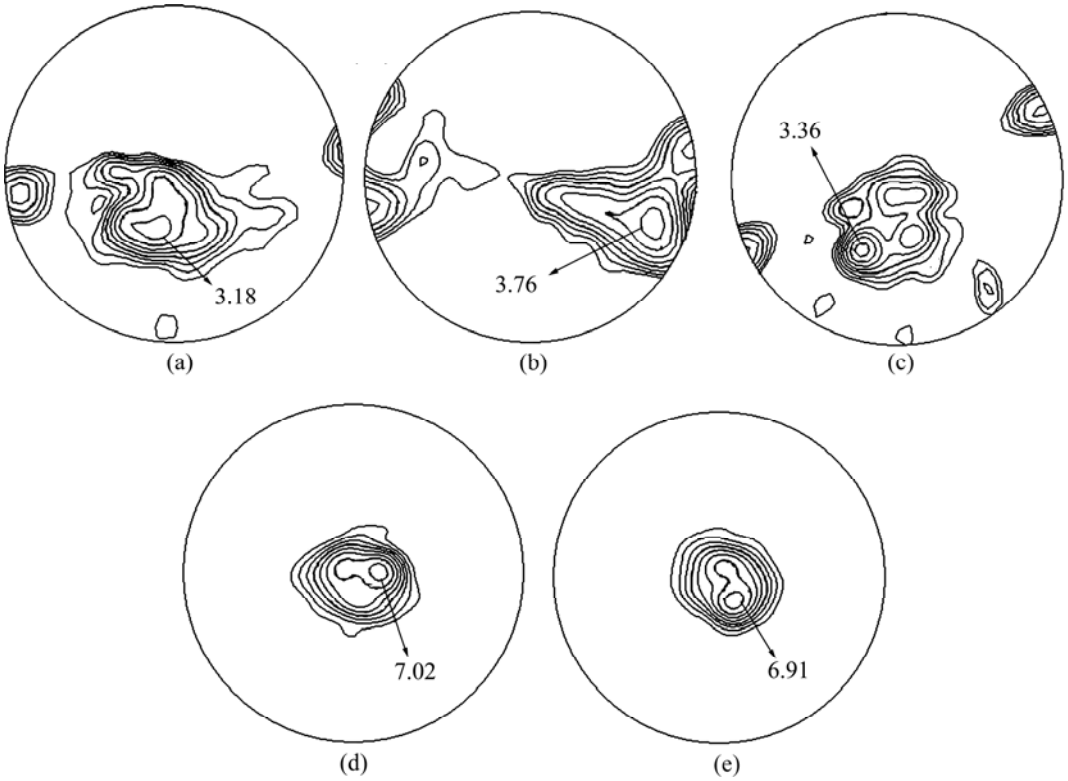

Fig.5 (0002) pole figures of WZ62 alloy processed by ECAE-one pass (a), ECAE-two passes (b), ECAE-three passes (c), E2F (d) and E3F (e) (The extrusion direction is to the up in Fig5(a)−(c), the forging direction is perpendicular to the ED-TD surface in Figs.5(d) and (e).)

similarity between the texture evolutions after ECAE was also reported in the AZ31 alloy with different initial states[16].

In order to compare the effect of different texture patterns on the mechanical properties, the simple schematic illustration of crystallographic orientations induced by different processing routes in the present study is presented in Fig.6. Notice that different crystallographic orientations with non-basal texture component were simplified and described as 45° to ED. It is generally accepted that basal slip is the dominate deformation mode in magnesium alloys at room temperature. When the ECAE processed specimen with texture Fig.6(a) is tensioned along the extrusion direction, easy basal slip would occur because the maximum shear force occurs on the plane inclined at 45° to the tensile direction. As a consequence, both the UTS and YS would be reduced and the elongation would be enhanced. If the samples were processed by forging in consequence, the basal planes were rotated to be normal to the ND (see Fig.6(b)), resulting in hard occurrence of the basal slip and increment in strength.

In the present study, ECAE followed by forging processing was developed to control the textures, aiming to change the mechanical properties of WZ62 alloy. If the parameters of the secondary forging processing (such as reduction) can be changed, and the final texture can also be controlled, resulting in difference in the mechanical properties.

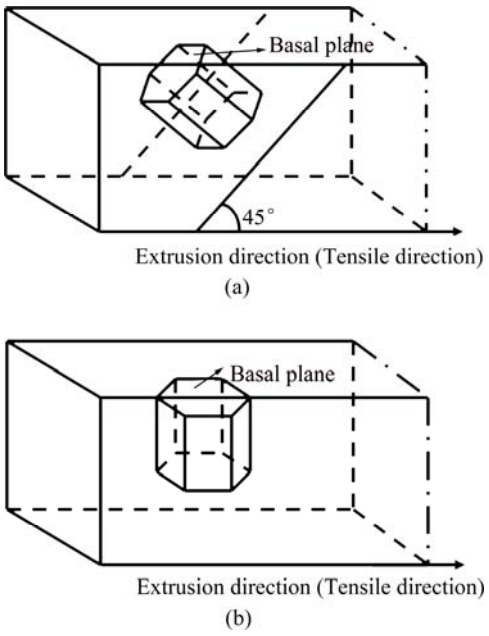

Fig.6 Schematic illustration of crystallographic orientations formed by ECAE (a) and ECAE followed by forging processing (b)

4 Conclusions

1) The “necklace” structure is found in the WZ62 alloys produced by ECAE, and ECAE followed by forging processing respectively. From the microstructure observation, it can be imaged that the DRX process may be associated with strain localization.

2) Both the ultimate tensile strength and yield strength are improved by the secondary forging processing followed by ECAE. The change in mechanical properties is attributable to the change in texture; after forging processing the majority of basal planes are inclined to be perpendicular to the normal direction, which is hard for basal slip.

3) From the texture analysis in the present study, the initial textures induced by ECAE make only a limited contribution to the ultimate texture, which is dominated by the secondary forging processing.

References

[1] KAWAMURA Y, HAYASHI K, INOUE A, MASUMOTO T. Rapidly solidified powder metallurgy Mg97Zn1Y2 alloys with excellent tensile yield strength above 600 MPa[J]. Materials Transaction, 2001, 42: 1172−1176.

[2] ABE E, KAWAMURA Y, HAYASHI K, INOUE A. Long-period ordered structure in a high-strength nanocrystalline Mg-1at% Zn- 2 at% Y alloy studied by atomic-resolution Z-contrast STEM[J]. Acta Materialia, 2002, 50: 3845−3857.

[3] LUO Z P, ZHANG S Q. High-resolution electron microscopy on the X-$Mg_{12}ZnY$ phase in a high strength Mg-Zn-Zr-Y magnesium alloy[J]. Journal Material Science Letter, 2000, 19: 813−815.

[4] ITOI T, SEIMIYA T, KAWAMURA Y, HIROHASHI M. Long period stacking structures observed in $Mg_{97}Zn1Y_2$ alloy[J]. Scripta Materialia, 2004, 51: 107−111.

[5] ZHU Y M, MORTON A J, NIE J F. The 18R and 14H long-period stacking ordered structures in Mg-Y-Zn alloys[J]. Acta Materialia, 2010, 58: 2936−2947.

[6] KAWAMURA Y, YOSHIMOTO S. High strength Mg-Zn-Y alloys with LPSO structure[J]. Magnesium Technology, 2005: 499−502.

[7] KAWAMURA Y, KASAHARA T, IZUMI S, YAMASAKI M. Elevated temperature Mg97Y2Cu1 alloy with long period ordered structure[J]. Scripta Materialia, 2006, 5: 453−456.

[8] KIM W J, JEONG H T. Grain-size strengthening in equal-channel-angular-pressing processed AZ31 Mg alloys with a constant texture[J]. Materials Transaction, 2005, 46: 251−258.

[9] PONGE D, GOTTSTEIN G. Necklace formation during dynamic recrystallization: mechanisms and impact on flow behavior[J]. Acta Materialia, 1998, 1: 69−80.

[10] AL-SAMMAN T, GOTTSTEIN G. Dynamic recrystallization during high temperature deformation of magnesium[J]. Materials Science and Engineering A, 2008, 490: 411−420.

[11] ZHOU L X, BAKER T N. Effects of strain rate and temperature on deformation behaviour of IN 718 during high temperature deformation[J]. Materials Science and Engineering A, 1994, 177: 1−9.

[12] WUSATOWSKA-SARNEK A M, MIURA H, SAKAI T. Nucleation and microtexture development under dynamic recrystallization of copper[J]. Materials Science and Engineering A, 2002, 323: 177−186.

[13] McQUEEN H J, KONOPLEVA E V. Creep and hot working of Mg alloy AZ91[J]. Magnesium Technology, 2001: 227−234.

[14] SUN D K, CHANG C P, KAO P W. Microstructural study of strain localization in hot compressed Mg-3Al-1Zn alloy[J]. Materials Science and Engineering A, 2010, 527: 7050−7056.

[15] GARCÉS G, MÜLLER A, OÑORBE E, PÉREZ P, ADEVA P. Effect of hot forging on the microstructure and mechanical properties of Mg-Zn-Y alloy[J]. Journal of Materials Processing Technology, 2008, 206: 99−105.

[16] AGNEW S R, MEHROTRA P, LILLO T M, STOICA G M, LIAW P K. Crystallographic texture evolution of three wrought magnesium alloys during equal channel angular extrusion[J]. Materials Science and Engineering A, 2005, 408: 72−78

加工路径对 WZ62 合金的织构和力学性能的影响

施斌卿, 陈荣石, 柯 伟

中国科学院 金属研究所 金属腐蚀与防护国家重点实验室, 沈阳 110016

摘 要：通过等通道挤压和等通道挤压加锻造的方法制备变形 Mg-6.6%Y-2.3%Zn (WZ62，质量分数)镁合金。通过组织观察发现了由细小的再结晶晶粒和粗大的初始晶粒组成的“项链组织”，这种动态再结晶的过程可能与应变局域化有关。拉伸实验结果表明：随着等通道道次的增加，强度和塑性都得到了提高；在(0002)极图中观察到一种基轴偏转约 45°的非基面织构成分。经过等通道挤压后的锻造加工，强度得到大幅度提高但塑性降低了。这与织构的变化有关：大部分基面都旋转到垂直于法线方向(锻造方向)。二次锻造加工可以改变初始等通道挤压引入的非基面织构。

关键词：镁合金；Mg-Y-Zn 合金；等通道挤压；织构控制；

(Edited by LI Xiang-qun)